ACS APPLIED ENERGY MATERIALS
Cite This: ACS Appl. Energy Mater. 2018, 1, 552−560
Article
www.acsaem.org

Synthesis of Fine Cubic $Li_7La_3Zr_2O_{12}$ Powders in Molten LiCl−KCl Eutectic and Facile Densification by Reversal of Li^+/H^+ Exchange

J. Mark Weller, Justin A. Whetten, and Candace K. Chan*

Materials Science and Engineering, School for Engineering of Matter, Transport and Energy, Arizona State University, Tempe, Arizona 85287-6106, United States

Supporting Information

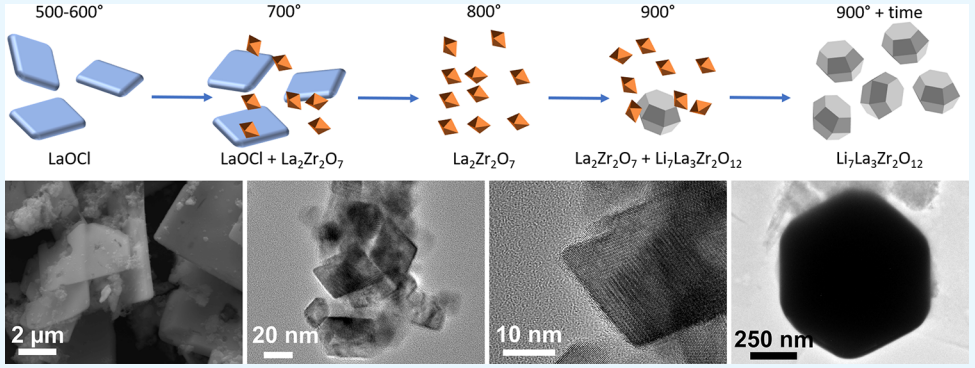

ABSTRACT: Recently, solid-state electrolytes have been a highly active area of research for future Li-ion batteries due to the potential for drastically improved energy density and safety. Among these materials, garnet structured lithium lanthanum zirconate ($Li_7La_3Zr_2O_{12}$, LLZO) shows particular promise owing to the high ionic conductivity of its cubic polymorph, inertness, and electrochemical stability against metallic lithium. Herein we report the facile preparation of phase-pure, cubic LLZO via molten salt synthesis in a eutectic mixture of LiCl−KCl at 900 °C. Fine powders of Al- and Ga-doped LLZO were obtained with primary particle sizes ranging from 0.3 to 3 μm. Depending on the consolidation conditions, pellets with up to 86% relative density could be obtained, with Li^+ conductivity values ranging from 0.230 to 0.371 mS cm^{-1}. It is also observed that while the effect of hydration has a profoundly deleterious effect on sintering and densification, this effect can be mitigated by the simple addition of LiOH before sintering to reverse hydration and aid densification. Qualitative discussions on the mechanisms of LLZO formation in the molten salt medium are discussed, in addition to implications for scalable processing of LLZO electrolytes.

KEYWORDS: *solid electrolyte, lithium ion conductor, molten salt synthesis, garnet, $Li_7La_3Zr_2O_{12}$ sintering*

1. INTRODUCTION

All-solid-state Li metal batteries containing solid electrolytes have the potential to offer higher energy densities and safety characteristics compared to those of conventional Li-ion batteries.[1,2] Among the various solid electrolytes, the garnet-type $Li_7La_3Zr_2O_{12}$ (LLZO) is one of the most promising ceramic Li-ion conductors due to its high ionic conductivity and chemical stability against both air and metallic lithium.[2,3]

Typically, LLZO is prepared via conventional solid-state reaction (SSR) using LiOH or Li_2CO_3, La_2O_3, and ZrO_2, along with oxides of dopants (e.g., Al_2O_3) as reagents.[3,4] This method generally requires high temperatures (>1100 °C) and/or long sintering times (24+ hours) to obtain powders with the desired crystal structure and ionic conductivity. The cubic phase of LLZO (c-LLZO, space group $Ia\bar{3}d$) generally displays high Li-ion conductivity on the order of 0.1−1 mS cm^{-1}, while the tetragonal phase (t-LLZO, space group $I4_1/acd$) has poor conductivity between 10^{-6} and 10^{-7} S cm^{-1}.[5] Typically, dopants are added to LLZO in order to stabilize the thermodynamically unfavorable cubic phase at room temperature. For example, Al(III), Ta(V), Nb(V), Mo(VI), and Ga(III) dopants are used to stabilize the cubic phase at room temperature along with conferring high Li-ion conductivity.[6−14]

For practical applications, the ability to synthesize LLZO at lower temperatures, in less time, and in forms other than bulk powders would be highly advantageous. To this end, many researchers have focused on low temperature synthesis methods, most frequently utilizing some variation of the sol−gel method.[7,15−19] Often, these methods are geared toward the preparation of nanosized LLZO particles, including our recent synthesis of undoped, size-stabilized c-LLZO using electrospinning[20] and nanocellulose templating.[21] Many of these techniques have been discussed in our recent review.[22] Another distinct approach is by use of thin-film deposition techniques, such as atomic layer deposition (ALD) or chemical vapor deposition (CVD), as outlined in works by Kazyak et al.[23] and

Received: November 9, 2017
Accepted: January 9, 2018
Published: January 9, 2018

DOI: 10.1021/acsaem.7b00133
ACS Appl. Energy Mater. 2018, 1, 552−560

Loho et al.,[24] respectively. These are promising techniques allowing low temperature deposition (555 °C[23] or 700 °C,[24] respectively) of thin, conformal films of LLZO. However, to date, the conductivity of these films is still rather low (~1.2 × 10^{-6} S cm^{-1} at 100 °C[23] and 4.2 × 10^{-6} S cm^{-1} for tetragonal LLZO at room temperature[24]), and more work needs to be done to minimize impurity phases and improve the performance.

While these various methods are successful, in general they do not confer an easily scalable method to form LLZO, given the typically high cost for sol−gel precursors (e.g., metal alkoxides) and large amounts of "sacrificial" reagents such as excess solvents (alcohols, glycols, etc.), combustible material (nanocellulose, polymers, or "Pechini method" type synthesis), or high vacuum equipment (for ALD, CVD, etc.). Among the various means to prepare nanocrystalline ceramics, molten salt synthesis (MSS) (sometimes known as "salt melt synthesis" or the "molten salt method") is a common method to obtain various-sized particles of ceramics from generally inexpensive precursors at temperatures or times lower than those required in SSR.[25−32] In MSS, precursors usually consisting of metal oxides or metal salts are mixed intimately with a salt (or salt mixture, often a eutectic), followed by heat treatment above the melting point of the salt(s) to provide the thermodynamic driving force for dissolution of the precursors and to promote the formation of the desired crystalline phase.[33]

While the MSS method has been utilized for quite some time to synthesize nanostructured oxides,[33] it has only been recently applied to the synthesis of LLZO. Reddy et al. utilized a eutectic mixture of lithium nitrate ($LiNO_3$) and lithium chloride (LiCl) as the molten medium, with lanthanum oxide, zirconium tetrachloride, and tantalum oxide as precursors for the synthesis of tantalum-doped LLZO (LLZTO) between 700 and 900 °C.[32] Aggregates of micrometer-sized, irregularly faceted crystals of LLZTO were obtained using this method. The resultant materials exhibited a maximum ionic conductivity value of 0.78 × 10^{-5} S cm^{-1} at room temperature, in contrast to the roughly 100× higher conductivity generally reported for LLZTO prepared using SSR.[8,34,35] The low ionic conductivity in the particles prepared using this MSS method was attributed to the postsynthesis, aqueous washing step used to remove the eutectic salt medium, which led to an exchange of Li^+ with protons.[30]

In this work, we explore the synthesis of LLZO in a eutectic mixture of lithium chloride and potassium chloride (59:41 mol % LiCl:KCl) to further develop the use of MSS to obtain LLZO powders in large quantities, and examine the thermodynamic and kinetic factors affecting the formation of LLZO in this medium. In addition to forming c-LLZO without the requirement of extrinsic dopants, aluminum-doped (ALLZO) and gallium-doped (GLLZO) LLZO powders were also easily synthesized using this approach. The role of proton-exchange and hydration on the sinterability of the as-synthesized powders was also investigated. We find that, in the case of ALLZO and GLLZO powders synthesized via MSS, ceramic pellets with reasonably high density and conductivities are obtained, and that the proton-exchange can be reversed through the incorporation of LiOH prior to pellet sintering.

2. EXPERIMENTAL SECTION

2.1. Materials and Reagents. All reagents used are of ACS grade or higher and used as-received. Lithium chloride (LiCl), potassium chloride (KCl), lithium nitrate ($LiNO_3$), zirconium oxynitrate ($ZrO(NO_3)_2$) hydrate, aluminum nitrate ($Al(NO_3)_3$) nonahydrate, and gallium nitrate ($Ga(NO_3)_3$) hydrate were obtained from Sigma-Aldrich. Lanthanum nitrate ($La(NO_3)_3$) hexahydrate was obtained from Alfa Aesar.

2.2. Preparation of LLZO Salt Precursor Mixtures. To prepare the chloride salt mixture, 59 mol % LiCl and 41 mol % KCl were mixed followed by grinding thoroughly with a mortar and pestle. The LLZO nitrate precursors were prepared by mixing $LiNO_3$, $La(NO_3)_3$, and $ZrO(NO_3)_2$ in a 7:3:2 molar ratio and grinding thoroughly with a mortar and pestle. In the case of ALLZO, Al^{3+} from $Al(NO_3)_3$ was used as a substitutional dopant for Li^+ to introduce the critical level of Al-doping (i.e., greater than 0.204)[36] to stabilize the cubic phase of LLZO, resulting in a nominal formula of $Li_{6.28}Al_{0.24}La_3Zr_2O_{12}$. Similarly, in the case of GLLZO, $Ga(NO_3)_3$ was used to introduce a critical level of Ga-doping,[13] resulting in a nominal formula of $Li_{6.25}Ga_{0.25}La_3Zr_2O_{12}$.

2.3. Molten Salt Synthesis of LLZO. Before heat treatment, the chloride salt mixture and the nitrate precursor salt mixture were mixed by grinding thoroughly with a mortar and pestle and then added to alumina crucibles. The premixed chloride salts and precursor salts were mixed in a 1:1 ratio by mass, with total mass between 2 and 4 g for exploratory syntheses, and up to 50 g for producing large batches for densification and ionic conductivity studies. The crucibles were covered with alumina lids to mitigate the evaporation of salts at high temperatures. Since the salt mixture melts at 352 °C,[33] temperatures between 500 and 900 °C were readily accessible for experimentation to determine optimal reaction conditions. In general, the mixtures were heated at a rate of 5 °C/min (Thermo Scientific Lindberg Blue M), held for various times (between 1−6 h), and cooled naturally to room temperature in the furnace.

After the synthesis, ultrapure water (>18 MOhm cm) was added to the cooled crucibles, and the suspension was ultrasonicated using an immersion probe (Cole-Parmer 500 W Ultrasonic Processor) to rapidly dissolve the fused salts and generate a slurry of powder. Subsequently, the slurry was vacuum filtered using poly(vinylidene fluoride) membranes (0.22 μm pore size, DuraPore, EMD corporation) and washed with at least 150 mL of water followed by 50 mL of methanol (BDH, HPLC grade) to facilitate fast drying. Finally, the filter membranes along with the wet powder cakes were placed in an oven at 50 °C and dried in air. After drying, the powders were removed from the filter membranes and lightly ground with a mortar and pestle.

2.4. Ceramic Pellet Preparation. LLZO pellets were consolidated from the as-synthesized powders via uniaxial cold-pressing (SpecAc Atlas 15T Manual Hydraulic Press) using a 6 mm stainless steel die. Before pressing, powders were crushed using a mortar and pestle followed by vibratory ball-milling (SPEX Corporation, 8000M) for 5 min to help mitigate agglomeration of particles. Optionally, 3% or 10% (by mass) LiOH was added. Pellets were pressed using 2 t of force for 5 min.

All pressed green pellets were sintered at 1100 °C for between 6 and 18 h. For sintering, pellets were placed on a bed of mother powder and covered with additional mother powder to offset lithium loss. All pellets were supported on a MgO plate that was placed inside of an alumina crucible (CoorsTek) in order to prevent both adventitious aluminum doping and sticking of the LLZO pellets to the crucible.[6] Further, 100−200 mg of lithium carbonate were also placed within the alumina crucible, adjacent to the pellets, to generate a lithium-rich vapor-phase during sintering. All crucibles were covered with an alumina lid (CoorsTek) during sintering. A representative photograph of this arrangement can be seen in Figure S1. The density of the pellets was calculated from the sample geometry and mass and compared to the theoretical density of Al- and Ga-doped LLZO (5.107 g cm^{-3}).[6,14,37]

2.5. Materials Characterization. X-ray diffraction (XRD) was performed using a Siemens D5000 powder diffractometer with Cu Kα radiation for phase identification. The reference pattern for c-LLZO ($Ia\bar{3}d$) was generated according to the structure reported by Geiger et al.[37]

DOI: 10.1021/acsaem.7b00133
ACS Appl. Energy Mater. 2018, 1, 552−560

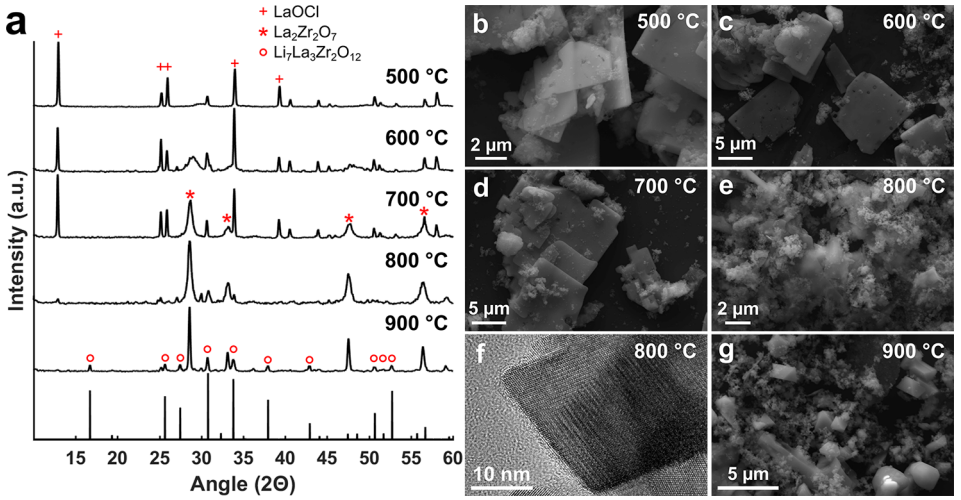

Figure 1. Formation process of LLZO using different reaction temperatures (500−900 °C) and 3 h hold times. (a) XRD patterns (c-LLZO reference structure from ref 37 on bottom); (b−g) respective SEM or TEM images showing morphology of materials synthesized at various temperatures.

The sample morphology was examined using an FEI XL30 scanning electron microscope (SEM) equipped with an EDAX system, or an FEI Nova 200 dual-beam SEM-FIB with a Thermo Scientific solid-state energy dispersive spectrometer. Transmission electron microscopy (TEM) was performed using an FEI Titan Environmental TEM operated at 300 kV. To prepare TEM samples, the LLZO powder was ultrasonically suspended in methanol. A holey carbon TEM grid (Pacific Grid Tech) was then briefly immersed into the aforementioned suspension. Crystalmaker Single Crystal software was used to simulate the selected area diffraction pattern (SADP) of c-LLZO based on the structure from Geiger et al.[37]

2.6. Ionic Conductivity Measurements. After sintering, the dense pellets were polished using 400 grit alumina polishing films (Agilent) until a smooth, uniform surface was obtained. Metal contacts were applied by sputter coating a ∼10 nm Au film onto the polished surfaces. Symmetric cells with the Au electrodes were analyzed via electrochemical impedance spectroscopy (EIS) using a BioLogic SP200 potentiostat. Impedance spectra were recorded from 1 kHz to 7 MHz at room temperature and fit (Supporting Information) using the Z fit analysis tool in the BioLogic EC-lab software.

3. RESULTS AND DISCUSSION

3.1. Characterization and Discussion of Formation Mechanism. In the method reported by Reddy et al., a eutectic mixture of $LiNO_3$ and LiCl (88:12 mol %, mp ∼280 °C) was used to synthesize LLZTO between 700 and 800 °C.[32] While effective for preparing LLZO, the products obtained in this method had two undesirable properties. First, the pellets formed from these powders had uncharacteristically low Li^+ ionic conductivity, as previously mentioned. This is likely explained by the well-known Li^+/proton-exchange effect that is noted when LLZO is exposed to water or moist air, which has a negative effect on conductivity.[38−40] Second, the morphology of the as-synthesized powders was somewhat irregular, whereas MSS commonly produces more uniform powders. The latter is likely explained as follows: due to the boiling and/or decomposition of $LiNO_3$ at around 600 °C,[41] there is a high possibility that some, if not much, of the nitrate portion of the medium evaporates under conditions (i.e., temperatures between 700 and 800 °C) that form LLZTO. The evaporation of a substantial portion of the reaction medium could have a deleterious effect on the uniformity and morphology of the resultant powders.

To mitigate this challenge, our approach utilizes less volatile salt species, specifically, a eutectic mixture of LiCl−KCl[33] (59:41 mol %, mp ∼352 °C; LiCl bp ∼1382 °C, KCl bp ∼1420 °C, compared to ∼600 °C for $LiNO_3$[41]). In this case, since the molten chloride medium contains no innate oxygen source (besides the slow diffusion of atmospheric oxygen), precursors that can provide reactive oxygen species are required. Therefore, a stoichiometric mixture of $LiNO_3$, $La(NO_3)_3$, and $ZrO(NO_3)_2$ was chosen to provide reactive oxoanions while also forming a completely homogeneous salt melt from which to precipitate fine oxide powders. Although LiCl may provide the Li^+ needed to form LLZO, $LiNO_3$ was also added in order to ensure that enough reactive oxygen species could be generated upon decomposition of the NO_3^- anion (eq 1) to react with all metal cations:

$$4NO_3^- \rightarrow 2O^{2-} + 4NO_2 + O_2 \quad (1)$$

In short, the excess $LiNO_3$ ensures that more than enough oxygen is provided to the system to generate stoichiometric LLZO. In contrast to Reddy and co-workers' use of oxides for some of the precursors, all salt precursors were chosen herein so that potential concentration gradients due to dissolution and diffusion of the metal oxides were eliminated. This is to aid the formation of a smaller particle size distribution and ensure initial homogeneity of all species in the reaction mixture.

A large design space was investigated to elucidate some of the thermodynamic and kinetic factors involved in formation of LLZO in this system, and is summarized in Table S1 and Figure S2. Selected XRD patterns showing the phases present using different reaction temperatures (500−900 °C) and 3 h reaction time are displayed in Figure 1a.

When using an MSS reaction temperature of 500 °C, the only crystalline phase formed is lanthanum oxychloride (LaOCl), presenting as large plates with edge lengths on the order of several micrometers and thicknesses below several hundred nanometers (Figure 1b). This is unsurprising, as MSS was used to synthesize LaOCl plates by Huang et al. at temperatures between 300 and 800 °C in molten LiCl−KCl eutectic.[42] Interestingly, no obvious evidence of crystalline zirconium containing phases was observed at 500 °C, indicating that most likely all of the La existed in the form of LaOCl. That said, several very broad features in the baseline of the XRD

DOI: 10.1021/acsaem.7b00133
ACS Appl. Energy Mater. 2018, 1, 552−560

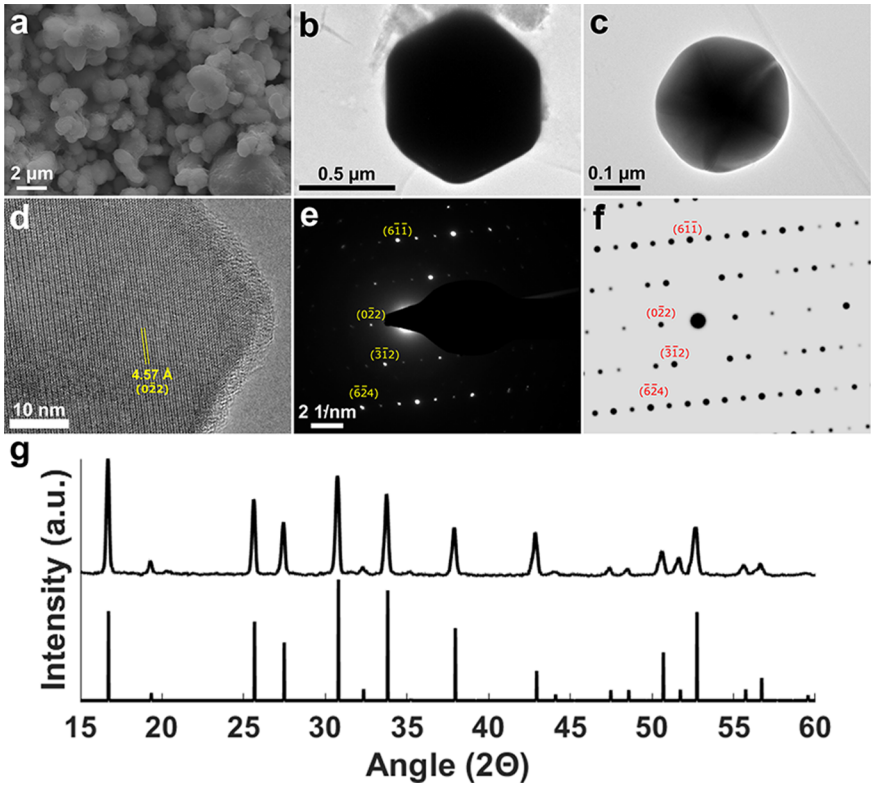

Figure 2. Phase-pure c-LLZO powders synthesized via MSS without added dopants (4 h reaction at 900 °C): (a) SEM image of c-LLZO with particle sizes between 0.3 and 3 μm, showing textured surfaces; (b, c) TEM images showing faceted particles of c-LLZO; (d) HRTEM image of particle edge from ball-milled (i.e., fractured) powder in (133) zone-axis orientation, (0$\bar{2}$2) lattice spacing noted; (e) parallel-beam nanodiffraction pattern of part d; (f) simulated (133) zone-axis SADP of c-LLZO using Crystalmaker Single Crystal software, based on the reference pattern generated according to Geiger et al.;[37] (g) powder XRD pattern (15−60°) of c-LLZO with reference pattern (Geiger et al.).[37]

pattern from the reaction conducted at 500 °C coincide with $La_2Zr_2O_7$ (LZO) peak positions, which may indicate that LZO is beginning to form even at this temperature. LZO is a known intermediate phase in LLZO sol−gel based syntheses and converts to LLZO upon reaction with additional Li.[20,21] Increasing the reaction temperature to 600 °C results in the formation of ultrafine (as indicated by extremely wide XRD peaks) LZO nanocrystals in addition to LaOCl plates (Figure 1c). At a reaction temperature of 700 °C, both phases still coexist, with the LZO reflections becoming somewhat sharper in the XRD patterns, indicating crystallite growth and/or an increasing degree of crystallization. As the temperature increases to 800 °C, the majority of LaOCl is consumed in favor of LZO, presenting as octahedral particles 30−40 nm across (Figure 1e,f). Interestingly, the LaOCl obtained at 800 °C by Huang et al.[42] presented in the form of nanoplates of similar morphology to our materials, indicating that the thermodynamic driving force in our case is the energetic favorability of another phase (i.e., LZO or LLZO) rather than the instability/solubility of LaOCl at 800 °C. This is suggested by the fact that nearly all LaOCl is gone at 800 °C and no LaOCl exists at 900 °C, with the implication that above a threshold temperature between 800 and 900 °C, all LaOCl has redissolved, providing soluble La-species necessary to form LLZO from nanocrystalline LZO. At 900 °C, a mixture of LZO and LLZO forms in 3 h (Figure 1g), and both very fine powders as well as highly faceted particles with side lengths between 0.5 and 2 μm can be seen.

Phase-pure c-LLZO was obtained using a reaction time of 6 h at 900 °C (Table S1). Optimization of the reaction time also resulted in phase-pure c-LLZO at 4 h at 900 °C (Figure 2), indicating that all LZO present after 3 h at 900 °C converts within 1 h to LLZO. As seen in Figure 2, LLZO particles formed in this 4 h reaction present either as faceted discrete particles (Figure 2b,c), or as spheroidal particles that may result from fusion of individual particles that come into contact in the melt (Figure 2a). Of note, the ability to synthesize faceted, submicron single crystals of LLZO may allow further investigation into the size-stabilization effect of undoped c-LLZO investigated by Yang et al.[20] and Gordon et al.[21] On the basis of the substantially larger size of the LLZO particles relative to the LZO nanocrystals, it is likely that an Ostwald ripening or similar process occurs, in which some LZO nuclei convert to LLZO while nearby nuclei below a size threshold are consumed in favor of larger LLZO particles. A fragmented (from high energy ball-milling) crystal of LLZO is shown in the HRTEM image in Figure 2d, with electron diffraction patterns shown in Figure 2e (measured) and Figure 2f (simulated based on data from Geiger et al.[37]). Observation of clear lattice fringes corresponding to the (0$\bar{2}$2) plane along with reflections corresponding solely to the [133] zone-axis diffraction pattern of LLZO indicates that at least some of the formed LLZO particles are single crystalline. This taken in conjunction with the observed faceted particles may further allude to an Ostwald ripening process.

In short, as the temperature and/or reaction time increase, the otherwise stable LaOCl begins to dissolve to form ultrafine LZO nanocrystals, followed by complete dissolution of LaOCl and formation of c-LLZO at 900 °C. This process is depicted in Scheme 1. Under optimized conditions wherein pure c-LLZO

DOI: 10.1021/acsaem.7b00133
ACS Appl. Energy Mater. 2018, 1, 552−560

Scheme 1. Overall Process of Formation of c-LLZO in Eutectic LiCl–KCl

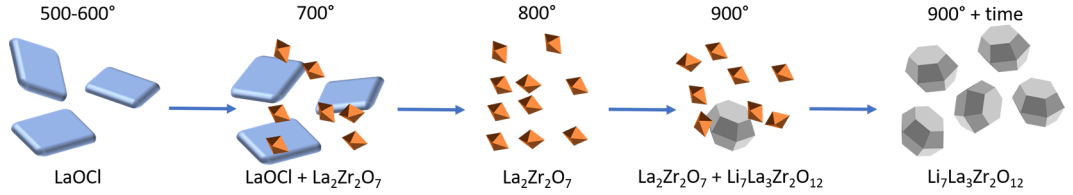

is obtained with a smaller particle size distribution (5 °C/min ramp to 900 °C, 4 h hold), phase-pure c-LLZO can be obtained without added extrinsic dopants. In this case, phase-pure c-LLZO particles with sizes primarily ranging from ~0.3 to 3 μm were obtained, with a mean and median particle size of 1.06 and 0.806 μm, respectively (Figure S3). This is consistent with our prior observations on nanostructured LLZO,[20,21] wherein c-LLZO formation is preferred in smaller particles. Further, in all cases of these exploratory MSS experiments, no dopants were added, suggesting that the particle/crystallite size of the LLZO formed under these conditions was below a critical threshold for size-stabilization.

In addition, Al-doped LLZO and Ga-doped LLZO (ALLZO and GLLZO, respectively) are easily obtained by addition of either $Al(NO_3)_3$ or $Ga(NO_3)_3$ to the salt precursor mixture. In each case, c-LLZO was obtained using the same reaction conditions as those used to obtain c-LLZO without added dopants, indicating that this method may be easily extended to incorporate a wide range of dopants. Representative SEM images of the as-synthesized doped powders and XRD patterns are depicted in the insets of Figure 3a,c and Figure 4 b,e, respectively. In addition, energy-dispersive X-ray spectroscopy (EDS) maps taken of these large batches of ALLZO (Figure S4) and GLLZO (Figure S5) indicated that the dopants are uniformly distributed throughout the as-synthesized powders. Large batches (~5–10 g) of the Al-doped, Ga-doped, and undoped c-LLZO were synthesized for subsequent densification studies and ionic conductivity measurements.

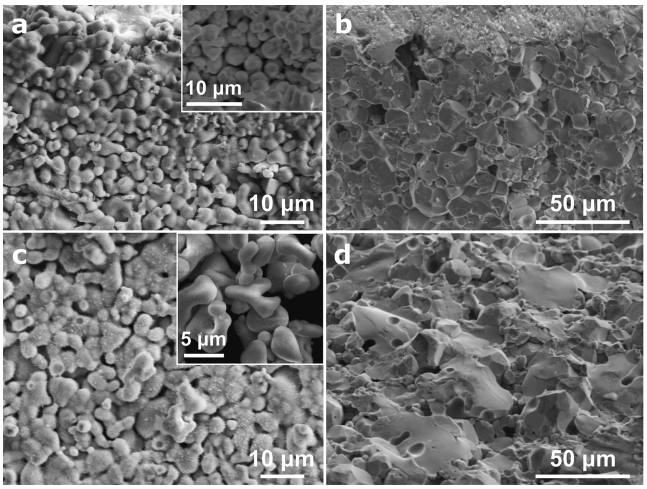

Figure 3. SEM images of fracture surfaces of (a) ALLZO pellet sintered without added LiOH for 18 h; (a inset) as-synthesized ALLZO powder; (b) ALLZO pellet sintered with 10% excess LiOH for 18 h; (c) GLLZO pellet sintered without added LiOH for 18 h; (c inset) as-synthesized GLLZO powder; (d) GLLZO pellet sintered with 10% excess LiOH for 12 h.

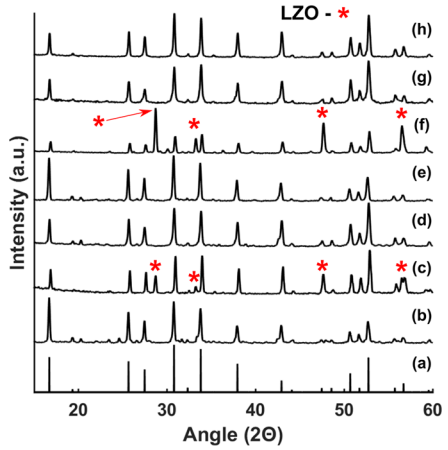

Figure 4. Comparison of XRD patterns of (a) c-LLZO reference pattern (from Geiger et al.),[37] (b) as-synthesized ALLZO powder, (c) ALLZO pellet without added LiOH sintered for 18 h, (d) ALLZO pellet sintered with 10% excess LiOH for 18 h, (e) as-synthesized GLLZO powder, (f) GLLZO pellet without added LiOH sintered for 18 h, (g) GLLZO pellet sintered with 10% excess LiOH for 12 h, and (h) GLLZO pellet sintered with 3% excess LiOH for 6 h. *LZO = $La_2Zr_2O_7$.

3.2. Densification and Conductivity of Sintered Powders. Pellets formed using the as-synthesized powders generally had quite poor properties. In general, the resultant densities were less than 50% of the theoretical density of c-LLZO, and XRD patterns of the pellets indicated some decomposition of LLZO to LZO (see Figure 4c,f), which is known to occur when LLZO becomes too Li-deficient.[17,43−45] Additionally, attempts to polish these pellets resulted in rapid abrasion of powder from the pellets, indicating that little to no sintering had occurred, even when heating at 1100 °C for 18 h. Because of this, only very noisy EIS spectra (not shown) could be obtained, with very large values of impedance. This phenomenon was observed in the undoped, Al-doped, and Ga-doped LLZO, and may be explained by the substantial hydration that most probably occurs during washing of the powders due to formation of Li_2CO_3. Cheng et al. and Sharafi et al. have demonstrated computationally that upon exposure to moisture, Li_2CO_3 formation is thermodynamically favorable at room temperature.[39,40] This may occur via a proton-exchange pathway[40] or by simple removal of Li^+ from the lattice, creating Li-deficient LLZO via formation of LiOH and subsequent reaction with CO_2 to form Li_2CO_3.[39] Hydration, proton-exchange, and doping with CO_2 have been demonstrated to separately displace Li^+ from LLZTO by Wang and Lai, with deleterious effects on conductivity.[46] In these cases and in the study by Larraz et al.,[38] only gaseous H_2O was discussed, and it can be assumed that liquid H_2O (used to wash the as-synthesized powders) will have a stronger propensity to induce protonation/hydration. Indeed, Shimonishi et al. demonstrated that, upon exposure to several aqueous solutions, LLZO pellets

DOI: 10.1021/acsaem.7b00133
ACS Appl. Energy Mater. 2018, 1, 552–560

show both a change in morphology and substantially reduced conductivity.[7] This strongly implies that the as-synthesized powders produced herein and by Reddy et al.[32] are negatively affected by exposure to water during washing.

In order to confirm whether or not hydration is the cause of the poor pellet properties, 3% or 10% (by mass) LiOH was added to the as-synthesized powder, followed by ball-milling for 5 min to intimately mix the powders and then subsequent pressing and sintering. LiOH (mp ~462 °C) easily forms an alkaline flux during sintering that should readily reverse proton-exchange if present, with the formation of water vapor, according to eq 2:

$$\mathrm{LiOH(l) + Li_{(7-x)}H_xLa_3Zr_2O_{12} \rightarrow Li_7La_3Zr_2O_{12} + xH_2O(g)} \quad (2)$$

In the case of powders with added LiOH, reasonably well-densified pellets (84−86% of theoretical density) were obtained unlike those prepared from only as-synthesized powder. All of the Nyquist plots for the well-densified ALLZO and GLLZO pellets displayed a tail at low frequencies, corresponding to the impedance at the electrodes, and a partial, slightly depressed semicircle at high frequencies attributed to the bulk conductivity (Figure 5). A second semicircle arising from the grain boundary resistance was not noticeable, which is often the case for LLZO pellets measured at room temperature. More importantly, fitting of the impedance data (Supporting Information, Table S2) showed that these pellets had ionic conductivities between 0.230 and 0.371 mS cm^{-1} (Table 1). This indicates that proton-exchange was reversed, as it is well-known that the proton-exchanged, "low-temperature cubic LLZO" has poor ionic conductivity.[38,47]

The fracture surfaces for the ALLZO (Figure 3a,b) and GLLZO (Figure 3c,d) pellets were characterized with SEM imaging. Figure 3a,c confirms that, for both ALLZO and GLLZO pellets prepared without added LiOH, little sintering had occurred, as the particle morphology is nearly the same as that of the as-synthesized powders (shown in the insets). Only slight coalescence of the particles can be seen, with little reduction of void space or porosity. In contrast, Figure 3b,d illustrates significant sintering and grain coarsening, with a predominantly transgranular fracture observed, indicating substantially improved mechanical properties. However, spheroidal voids within grains as well as larger intergranular voids are observed in the well-densified samples. There are several possible explanations for this observation: First, it may be that the sintering time and/or temperature are not yet optimized for these powders, and it is entirely plausible that the reactions that occur when hydration is reversed cause some different behavior during sintering relative to conventionally synthesized powders. Second, a relatively large amount of LiOH was added, which while necessary to reverse protonation, may also result in residual voids after the excess LiOH evaporates during sintering. EDS maps of the fracture surfaces of ALLZO and GLLZO are shown in Figures S6 and S7, respectively, indicating that the distribution of dopants is still uniform, although it is possible that some Al-rich phases are present in the ALLZO case.

The density and ionic conductivity of our materials are slightly lower than those of the best ALLZO and GLLZO pellets prepared from powders synthesized using other methods (Table 1). That said, the conductivity values are within the expected values for c-LLZO, and in the case of ALLZO, our material exhibited higher conductivity than that of Yi et al.[19] even though it has noticeably lower density. Similarly,

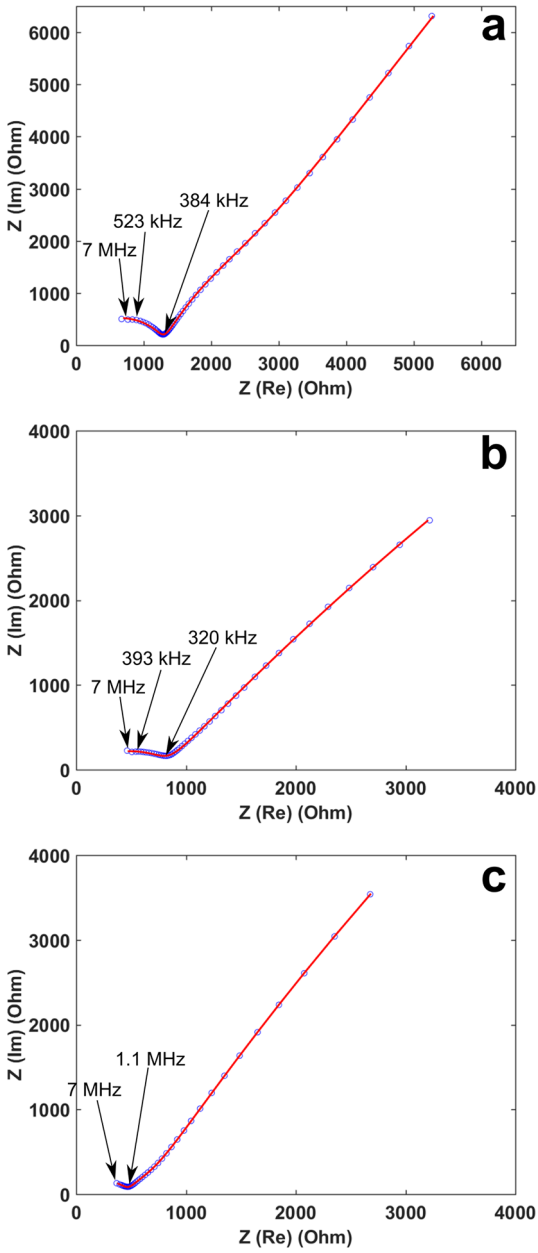

Figure 5. EIS spectra of (a) ALLZO pellet (sintered with 10% LiOH for 18 h) and (b, c) GLLZO pellets (sintered with 10% LiOH for 12 h and 3% LiOH for 6 h, respectively); the experimental data are plotted as circles and the solid line indicates the fit data.

our GLLZO has higher conductivity than that prepared by Wolfenstein et al.,[13] despite the lower density, and both conductivity and density compare favorably with GLLZO prepared via combustion synthesis by Afyon et al.[48] Taken in context, these initial results indicate that c-LLZO prepared via MSS can be processed in such a way to produce expected behavior as long as hydration can be reversed. While other researchers have demonstrated substantially higher conductivity for GLLZO (e.g., Yi et al.),[14] the relatively low density and clear existence of nonoptimized sintering as shown in Figure 3 indicate that, under fully optimized conditions, the materials synthesized here could have better dopant incorporation, higher density, and improved conductivity comparable to some of the more successful methods shown in Table 1.

DOI: 10.1021/acsaem.7b00133
ACS Appl. Energy Mater. 2018, 1, 552−560

Table 1. Comparison of Pellet Density and Room Temperature Total Ionic Conductivity for Al- and Ga-Doped LLZO Prepared Using Different Synthesis Methods

synthesis method (pellet sintering conditions)	relative density	ionic conductivity (mS cm^{-1})	ref
Al-Doped LLZO			
molten salt [as-synthesized] (1100 °C, 18 h)	<50%	n/a	this work
molten salt + 10 wt % LiOH (1100 °C, 18 h)	84%	0.230	this work
solid-state reaction (1300 °C, 1 h)	not reported	0.31	11
sol−gel (1100 °C, 1 h under 40 MPa)	96%	0.4	18
flame-spray (1090 °C, 1 h)	94%	0.2	19
Ga-Doped LLZO			
molten salt [as-synthesized] (1100 °C, 18 h)	<50%	n/a	this work
molten salt + 3 wt % LiOH (1100 °C, 6 h)	84%	0.371	this work
molten salt + 10 wt % LiOH (1100 °C, 12 h)	86%	0.323	this work
solid-state reaction (1000 °C, 1 h under 40 MPa)	91%	0.35	13
sol−gel (950 °C, 6 h)	76−80%	0.24	48
flame-spray (1130 °C, 0.3 h)	95%	1.3	14

3.3. Discussion of Densification and the Effect of Protonation/Hydration. As hydration is the most likely explanation for the low conductivity of the Ta-doped LLZO prepared via MSS by Reddy and co-workers,[32] the facile ability to reverse hydration/proton-exchange demonstrated here is an important result to motivate further exploration of MSS for the synthesis of LLZO. Recently, Yi et al. reported that hydration in the case of ALLZO and GLLZO powders synthesized via flame-spray pyrolysis actually aided in the densification of LLZO.[14] They theorize that hydration introduces additional mechanisms for densification, which operate in addition to conventional surface and bulk diffusion during sintering.[14] While this result is in clear contrast to our findings at first glance, the results may be reconciled as follows: in the case of flame-made powders with high specific surface areas, substantial hydration is unsurprising, especially when these powders are ball-milled for an extended time in air. However, all or nearly all of the Li^+ from the LLZO lattice that is displaced by either H^+/H_2O or reaction with CO_2 is still present as surface Li_2CO_3. In our case, the process of washing with a large volume of water to remove the salt media likely results in the gradual dissolution and removal of any LiOH or Li_2CO_3 that forms as a consequence of proton-exchange from the as-synthesized powders. Since our LLZO powders are washed using a vacuum filtration apparatus, repeated additions of ultrapure water are used, shifting the equilibrium for the Li^+/H^+ exchange reaction further toward removal of Li^+ and resulting in a net effect of lowering the stoichiometric level of Li, since some amount of the surface Li-species will dissolve and be washed away during each repeated washing step. The conversion of LLZO to LZO in the pellets sintered without added LiOH, as illustrated in Figure 4c,f, further corroborates this explanation. On the basis of the evidence presented, the addition of LiOH is critical to reverse hydration and allow dense LLZO with high conductivity to be obtained. The use of nonaqueous solvents such as lower alcohols (e.g., methanol) for washing may be worth investigating in future studies.

Molten salt synthesis has not been extensively investigated for the preparation of LLZO until recently. Here, we show that it can provide particular benefits to the synthesis of LLZO, including lower reaction temperatures than those used in solid-state reaction (and often in less time), less expensive precursors than those used in sol−gel methods, and a straightforward synthesis route that enables the rapid preparation of fine crystalline powders in a short time. The ability to easily synthesize fine, nonagglomerated powders of LLZO via MSS may be a critical step to widespread utilization of LLZO as a solid electrolyte. Since ball-milling has limitations to particle size reduction,[14] these more uniform and fine powders may enable roll-to-roll processing of electrolyte materials, e.g., by tape-casting such as demonstrated by Yi et al.[14,19] (which requires a stable slurry of fine powder), and thus better incorporation into practical battery production methods. This factor in particular overcomes one of the primary challenges of using a brittle, crystalline ceramic as an electrolyte. Finally, on a lab scale alone, tens of grams of uniform c-LLZO can be easily obtained in a matter of hours using a single small furnace, indicating that this synthesis approach may confer a new easily scalable method of LLZO production, necessary for implementation in future solid-state lithium ion batteries.

4. CONCLUSIONS

Undoped, aluminum-doped, and gallium-doped c-LLZO were successfully synthesized using a novel molten salt synthesis route. As the reaction temperature increases from 500 to 900 °C, LaOCl is formed, followed by initial formation of ultrafine LZO nanocrystals, and finally fine LLZO powders at 900 °C in 4 h. Well-dispersed, fine (submicron to few micron) powders were obtained under optimized conditions. The hydration/proton-exchange resulting from the unavoidable washing step involved in molten salt synthesis was also observed here, and a simple solution via addition of LiOH before pellet sintering is presented. Well-densified pellets were obtained with Li-ion conductivity values ranging from 0.230 to 0.371 mS cm^{-1} using simple uniaxial pressing followed by sintering at 1100 °C, indicating that, under further optimized conditions, these powders will result in ceramic electrolytes with excellent properties. Finally, the ease with which fine powders can be obtained with this method may be a crucial step toward realistic processing of LLZO for scalable solid-state lithium batteries.

■ ASSOCIATED CONTENT

Supporting Information

The Supporting Information is available free of charge on the ACS Publications website at DOI: 10.1021/acsaem.7b00133.

Procedures for EIS fitting, tabulated data, XRD patterns, SEM images with EDS spectra/maps (PDF)

■ AUTHOR INFORMATION

Corresponding Author

*E-mail: candace.chan@asu.edu. Phone: (480) 727-8614.

ORCID

J. Mark Weller: 0000-0003-2056-8974

Candace K. Chan: 0000-0003-4329-4865

Notes

The authors declare no competing financial interest.

DOI: 10.1021/acsaem.7b00133
ACS Appl. Energy Mater. 2018, 1, 552−560

■ ACKNOWLEDGMENTS

This work was supported by the NSF CAREER award DMR 1553519. J.M.W. acknowledges support from an ASU Fulton Schools of Engineering Dean's Fellowship, and J.A.W. thanks the Fulton Undergraduate Research Initiative at ASU for funding. The authors thank C. L. Tsai and M. Finsterbusch from Forschungszentrum Jülich GmbH, Institute of Energy and Climate Research, Materials Synthesis and Processing (IEK-1), for helpful discussions. The authors gratefully acknowledge the use of facilities within the LeRoy Eyring Center for Solid State Science at Arizona State University.

■ REFERENCES

(1) Knauth, P. Inorganic Solid Li Ion Conductors: An Overview. *Solid State Ionics* **2009**, *180*, 911−916.
(2) Thangadurai, V.; Narayanan, S.; Pinzaru, D. Garnet-Type Solid-State Fast Li Ion Conductors for Li Batteries: Critical Review. *Chem. Soc. Rev.* **2014**, *43*, 4714−4727.
(3) Ramakumar, S.; Deviannapoorani, C.; Dhivya, L.; Shankar, L. S.; Murugan, R. Lithium Garnets: Synthesis, Structure, Li^+ Conductivity, Li^+ Dynamics and Applications. *Prog. Mater. Sci.* **2017**, *88*, 325−411.
(4) Murugan, R.; Thangadurai, V.; Weppner, W. Fast Lithium Ion Conduction in Garnet-Type $Li_7La_3Zr_2O_{12}$. *Angew. Chem., Int. Ed.* **2007**, *46*, 7778−7781.
(5) Awaka, J.; Kijima, N.; Hayakawa, H.; Akimoto, J. Synthesis and Structure Analysis of Tetragonal $Li_7La_3Zr_2O_{12}$ with the Garnet-Related Type Structure. *J. Solid State Chem.* **2009**, *182*, 2046−2052.
(6) Tsai, C. L.; Dashjav, E.; Hammer, E. M.; Finsterbusch, M.; Tietz, F.; Uhlenbruck, S.; Buchkremer, H. P. High Conductivity of Mixed Phase Al-Substituted $Li_7La_3Zr_2O_{12}$. *J. Electroceram.* **2015**, *35*, 25−32.
(7) Shimonishi, Y.; Toda, A.; Zhang, T.; Hirano, A.; Imanishi, N.; Yamamoto, O.; Takeda, Y. Synthesis of Garnet-Type $Li_{7-X}La_3Zr_2O_{12-1/2x}$ and Its Stability in Aqueous Solutions. *Solid State Ionics* **2011**, *183*, 48−53.
(8) Ishiguro, K.; Nemori, H.; Sunahiro, S.; Nakata, Y.; Sudo, R.; Matsui, M.; Takeda, Y.; Yamamoto, O.; Imanishi, N. Ta-Doped $Li_7La_3Zr_2O_{12}$ for Water-Stable Lithium Electrode of Lithium-Air Batteries. *J. Electrochem. Soc.* **2014**, *161*, A668−A674.
(9) Kim, Y.; Yoo, A.; Schmidt, R.; Sharafi, A.; Lee, H.; Wolfenstine, J.; Sakamoto, J. Electrochemical Stability of $Li_{6.5}La_3Zr_{1.5}M_{0.5}O_{12}$ (M = Nb or Ta) against Metallic Lithium. *Front. Energy Res.* **2016**, *4*, 1−7.
(10) Liu, X.; Li, Y.; Yang, T.; Cao, Z.; He, W.; Gao, Y.; Liu, J.; Li, G.; Li, Z. High Lithium Ionic Conductivity in the Garnet-Type Oxide $Li_{72-X}La_3Zr_{2-X}Mo_XO_{12}$ (X = 0−0.3) Ceramics by Sol-Gel Method. *J. Am. Ceram. Soc.* **2017**, *100*, 1527−1533.
(11) Matsuda, Y.; Sakamoto, K.; Matsui, M.; Yamamoto, O.; Takeda, Y.; Imanishi, N. Phase Formation of a Garnet-Type Lithium-Ion Conductor $Li_{7-3x}Al_xLa_3Zr_2O_{12}$. *Solid State Ionics* **2015**, *277*, 23−29.
(12) Ohta, S.; Kobayashi, T.; Asaoka, T. High Lithium Ionic Conductivity in the Garnet-Type Oxide $Li_{7-X}La_3(Zr_{2-X}, Nb_X)O_{12}$ (X = 0−2). *J. Power Sources* **2011**, *196*, 3342−3345.
(13) Wolfenstine, J.; Ratchford, J.; Rangasamy, E.; Sakamoto, J.; Allen, J. L. Synthesis and High Li-Ion Conductivity of Ga-Stabilized Cubic $Li_7La_3Zr_2O_{12}$. *Mater. Chem. Phys.* **2012**, *134*, 571−575.
(14) Yi, E.; Wang, W.; Kieffer, J.; Laine, R. M. Key Parameters Governing the Densification of Cubic-$Li_7La_3Zr_2O_{12}$ Li^+ Conductors. *J. Power Sources* **2017**, *352*, 156−164.
(15) Janani, N.; Ramakumar, S.; Dhivya, L.; Deviannapoorani, C.; Saranya, K.; Murugan, R. Synthesis of Cubic $Li_7La_3Zr_2O_{12}$ by Modified Sol-Gel Process. *Ionics* **2011**, *17*, 575−580.
(16) Kokal, I.; Somer, M.; Notten, P. H. L.; Hintzen, H. T. Sol−gel Synthesis and Lithium Ion Conductivity of $Li_7La_3Zr_2O_{12}$ with Garnet-Related Type Structure. *Solid State Ionics* **2011**, *185*, 42−46.
(17) Xie, H.; Li, Y.; Goodenough, J. B. Low-Temperature Synthesis of $Li_7La_3Zr_2O_{12}$ with Cubic Garnet-Type Structure. *Mater. Res. Bull.* **2012**, *47*, 1229−1232.
(18) Sakamoto, J.; Rangasamy, E.; Kim, H.; Kim, Y.; Wolfenstine, J. Synthesis of Nano-Scale Fast Ion Conducting Cubic $Li_7La_3Zr_2O_{12}$. *Nanotechnology* **2013**, *24*, 42005.
(19) Yi, E.; Wang, W.; Kieffer, J.; Laine, R. M. Flame Made Nanoparticles Permit Processing of Dense, Flexible, Li^+ Conducting Ceramic Electrolyte Thin Films of Cubic-$Li_7La_3Zr_2O_{12}$ (c-LLZO). *J. Mater. Chem. A* **2016**, *4*, 12947−12954.
(20) Yang, T.; Gordon, Z. D.; Li, Y.; Chan, C. K. Nanostructured Garnet-Type Solid Electrolytes for Lithium Batteries: Electrospinning Synthesis of $Li_7La_3Zr_2O_{12}$ Nanowires and Particle Size-Dependent Phase Transformation. *J. Phys. Chem. C* **2015**, *119*, 14947−14953.
(21) Gordon, Z. D.; Yang, T.; Morgado, G. B. G.; Chan, C. K. 101, Preparation of Nano- and Microstructured Garnet $Li_7La_3Zr_2O_{12}$ Solid Electrolytes for Li-Ion Batteries via Cellulose Templating. *ACS Sustainable Chem. Eng.* **2016**, *4*, 6391−6398.
(22) Chan, C. K.; Yang, T.; Weller, J. M. Nanostructured Garnet-Type $Li_7La_3Zr_2O_{12}$: Synthesis, Properties, and Opportunities as Electrolytes for Li-Ion Batteries. Electrochim. *Electrochim. Acta* **2017**, *253*, 268−280.
(23) Kazyak, E.; Chen, K. H.; Wood, K. N.; Davis, A. L.; Thompson, T.; Bielinski, A. R.; Sanchez, A. J.; Wang, X.; Wang, C.; Sakamoto, J.; Dasgupta, N. P. Atomic Layer Deposition of the Solid Electrolyte Garnet $Li_7La_3Zr_2O_{12}$. *Chem. Mater.* **2017**, *29*, 3785−3792.
(24) Loho, C.; Djenadic, R.; Bruns, M.; Clemens, O.; Hahn, H. Garnet-Type $Li_7La_3Zr_2O_{12}$ Solid Electrolyte Thin Films Grown by CO_2-Laser Assisted CVD for All-Solid-State Batteries. *J. Electrochem. Soc.* **2017**, *164*, A6131−A6139.
(25) Zhang, S. Low Temperature Synthesis of Complex Refractory Oxide Powders From Molten Salts. *J. Pakistan Mater. Soc.* **2007**, *1*, 49−53.
(26) Wang, X.; Zhu, Y.; Zhang, W. Preparation of Lanthanum Zirconate Nano-Powders by Molten Salts Method. *J. Non-Cryst. Solids* **2010**, *356*, 1049−1051.
(27) Rahman, M. M.; Wang, J. Z.; Hassan, M. F.; Chou, S.; Wexler, D.; Liu, H. K. Basic Molten Salt Process-A New Route for Synthesis of Nanocrystalline $Li_4Ti_5O_{12}$-TiO_2 Anode Material for Li-Ion Batteries Using Eutectic Mixture of $LiNO_3$-LiOH-Li_2O_2. *J. Power Sources* **2010**, *195*, 4297−4303.
(28) Guo, Q.; Li, S.; Wang, H.; Gao, Y.; Li, B. Molten Salt Synthesis of Nano-Sized $Li_4Ti_5O_{12}$ Doped with Fe_2O_3 for Use as Anode Material in the Lithium-Ion Battery. *RSC Adv.* **2014**, *4*, 60327−60333.
(29) Guo, Q.; Wang, Q.; Chen, G.; Shen, M.; Li, B. Molten Salt Synthesis of Different Ionic Radii Metallic Compounds Doped Lithium Titanate Used in Li-Ion Battery Anodes. *Mater. Trans.* **2017**, *58*, 383−389.
(30) Huang, Z.; Deng, X.; Liu, J.; Jiao, C. Preparation of $CaZrO_3$ Powders by a Microwave − Assisted Molten Salt Method. *J. Ceram. Soc. Jpn.* **2016**, *124*, 593−596.
(31) Zhong, X.; Chen, M.; Zhu, Y.; Zhang, P.; Xu, M.; Li, W. Layered Lithium-Rich Oxide Nanoparticles: Low-Temperature Synthesis in Mixed Molten Salt and Excellent Performance as Cathode of Lithium-Ion Battery. *Ionics* **2017**, *23*, 1955−1966.
(32) Reddy, M. V.; Adams, S. Molten Salt Synthesis and Characterization of Fast Ion Conductor $Li_{6.75}La_3Zr_{1.75}Ta_{0.25}O_{12}$. *J. Solid State Electrochem.* **2017**, *21*, 2921−2928.
(33) Liu, X.; Fechler, N.; Antonietti, M. Salt Melt Synthesis of Ceramics, Semiconductors and Carbon Nanostructures. *Chem. Soc. Rev.* **2013**, *42*, 8237.
(34) Buschmann, H.; Berendts, S.; Mogwitz, B.; Janek, J. Lithium Metal Electrode Kinetics and Ionic Conductivity of the Solid Lithium Ion Conductors " $Li_7La_3Zr_2O_{12}$ " and $Li_{7-x}La_3Zr_{2-x}Ta_XO_{12}$ with Garnet-Type Structure. *J. Power Sources* **2012**, *206*, 236−244.
(35) Thompson, T.; Wolfenstine, J.; Allen, J. L.; Johannes, M.; Huq, A.; David, I. N.; Sakamoto, J. Tetragonal vs. Cubic Phase Stability in Al - Free Ta Doped $Li_7La_3Zr_2O_{12}$ (LLZO). *J. Mater. Chem. A* **2014**, *2*, 13431−13436.
(36) Rangasamy, E.; Wolfenstine, J.; Sakamoto, J. The Role of Al and Li Concentration on the Formation of Cubic Garnet Solid Electrolyte

DOI: 10.1021/acsaem.7b00133
ACS Appl. Energy Mater. 2018, 1, 552−560

of Nominal Composition $Li_7La_3Zr_2O_{12}$. *Solid State Ionics* **2012**, *206*, 28−32.
(37) Geiger, C. A.; Alekseev, E.; Lazic, B.; Fisch, M.; Armbruster, T.; Langner, R.; Fechtelkord, M.; Kim, N.; Pettke, T.; Weppner, W. Crystal Chemistry and Stability of "$Li_7La_3Zr_2O_{12}$" garnet: A Fast Lithium-Ion Conductor. *Inorg. Chem.* **2011**, *50*, 1089−1097.
(38) Larraz, G.; Orera, a.; Sanjuán, M. L. Cubic Phases of Garnet-Type $Li_7La_3Zr_2O_{12}$: The Role of Hydration. *J. Mater. Chem. A* **2013**, *1*, 11419.
(39) Cheng, L.; Wu, C. H.; Jarry, A.; Chen, W.; Ye, Y.; Zhu, J.; Kostecki, R.; Persson, K.; Guo, J.; Salmeron, M.; Chen, G.; Doeff, M. Interrelationships among Grain Size, Surface Composition, Air Stability, and Interfacial Resistance of Al-Substituted $Li_7La_3Zr_2O_{12}$ Solid Electrolytes. *ACS Appl. Mater. Interfaces* **2015**, *7*, 17649−17655.
(40) Sharafi, A.; Yu, S.; Naguib, M.; Lee, M.; Ma, C.; Meyer, H. M.; Nanda, J.; Chi, M.; Siegel, D. J.; Sakamoto, J. Impact of Air Exposure and Surface Chemistry on Li−$Li_7La_3Zr_2O_{12}$ Interfacial Resistance. *J. Mater. Chem. A* **2017**, *5*, 13475−13487.
(41) Patnaik, P. *Handbook of Inorganic Chemicals*; McGraw-Hill: New York, NY, 2003.
(42) Huang, Z.; Zhang, H.; Zhang, S. Growth of Well-Developed LaOCl Microplates by Chloride Salt-Assisted Method. *CrystEngComm* **2017**, *19*, 2971−2976.
(43) Deviannapoorani, C.; Dhivya, L.; Ramakumar, S.; Murugan, R. Synthesis of Garnet Structured $Li_{7+x}La_3Y_XZr_{2-X}O_{12}$ (X = 0−0.4) by Modified Sol-Gel Method. *J. Sol-Gel Sci. Technol.* **2012**, *64*, 510−514.
(44) Baek, S. W.; Lee, J. M.; Kim, T. Y.; Song, M. S.; Park, Y. Garnet Related Lithium Ion Conductor Processed by Spark Plasma Sintering for All Solid State Batteries. *J. Power Sources* **2014**, *249*, 197−206.
(45) Huang, M.; Liu, T.; Deng, Y.; Geng, H.; Shen, Y.; Lin, Y.; Nan, C.-W. Effect of Sintering Temperature on Structure and Ionic Conductivity of $Li_{7-x}La_3Zr_2O_{12-0.5x}$ (x = 0.5 ∼ 0.7) Ceramics. *Solid State Ionics* **2011**, *204*, 41−45.
(46) Wang, Y.; Lai, W. Phase Transition in Lithium Garnet Oxide Ionic Conductors $Li_7La_3Zr_2O_{12}$: The Role of Ta Substitution and H_2O/CO_2 Exposure. *J. Power Sources* **2015**, *275*, 612−620.
(47) Toda, S.; Ishiguro, K.; Shimonishi, Y.; Hirano, A.; Takeda, Y.; Yamamoto, O.; Imanishi, N. Low Temperature Cubic Garnet-Type CO_2-Doped $Li_7La_3Zr_2O_{12}$. *Solid State Ionics* **2013**, *233*, 102−106.
(48) Afyon, S.; Krumeich, F.; Rupp, J. L. M. A Shortcut to Garnet-Type Fast Li-Ion Conductors for All-Solid State Batteries. *J. Mater. Chem. A* **2015**, *3*, 18636−18648.

DOI: 10.1021/acsaem.7b00133
ACS Appl. Energy Mater. 2018, 1, 552−560